Use of incipient motion data for backward erosion piping models

Vera M. van Beek, Bryant A. Robbins, Gijs J.C.M. Hoffmans, Adam Bezuijen, Leo C. van Rijn

www.elsevier.com/locate/ijsrc

PII: S1001-6279(17)30207-X
DOI: https://doi.org/10.1016/j.ijsrc.2019.03.001
Reference: IJSRC227

To appear in: *International Journal of Sediment Research*

Received date: 6 July 2017
Revised date: 14 February 2019
Accepted date: 11 March 2019

Cite this article as: Vera M. van Beek, Bryant A. Robbins, Gijs J.C.M. Hoffmans, Adam Bezuijen and Leo C. van Rijn, Use of incipient motion data for backward erosion piping models, *International Journal of Sediment Research,* https://doi.org/10.1016/j.ijsrc.2019.03.001

Use of incipient motion data for backward erosion piping models

Use of incipient motion data for backward erosion piping models

Vera M. van Beek[a,*], Bryant A. Robbins[b], Gijs J.C.M. Hoffmans[a], Adam Bezuijen[a,c], Leo C. van Rijn[d]

[a]Deltares,Boussinesqweg 1,2629 HV Delft, The Netherlands
[b]U.S. Army Corps of Engineers, 3909 Halls Ferry Road,Vicksburg, MS 39180
[c]Ghent University,Technologiepark Zwijnaarde 905,9052 Zwijnaarde, Belgium
[d]Domineeswal 6, 8356 DS Blokzijl, The Netherlands

[*]Corresponding author:+31 (0)615838512; vera.vanbeek@deltares.nl

ABSTRACT

Backward erosion piping involves the gradual removal of granular material under the action of water flow from the foundation of a dam or levee, whereby shallow pipes are formed that grow in the direction opposite to the flow. This pipe-forming process can ultimately lead to failure of a water-retaining structure and is considered one of the most important failure mechanisms for dikes and levees in the Netherlands and the United States. Modeling of this mechanism requires the assessment of hydraulic conditions in the pipe, which are controlled by the particle equilibrium at the pipe wall. Since the pipe's dimensions are controlled by the inflow to the pipe from the porous medium, the flow through the pipe is thought to be laminar for fine- to medium-grained sands. The literature provides data for incipient motion in laminar flow, which is reviewed here and complemented with data from backward erosion experiments. The experiments illustrate the applicability of the laminar incipient motion data to determine the erosion pipe dimensions and corresponding pipe hydraulics for fine- to medium-grained sands, for the purpose of backward erosion piping modeling.

Keywords: Internal erosion, Backward erosion piping, Cylindrical test, Incipient motion, Dikes, Levees

List of Symbols

a	radius in vertical direction in an ellipse [m]
b	radius in horizontal direction in an ellipse [m]
C	coefficient of percolation in Bligh's rule [-]
d	particle diameter [m]
d_x	grain diameter for which *x*% of the sample (by weight) is finer [m]
g	gravitational acceleration [m/s^2]
h	pipe depth in infinitely wide pipe [m]
H	head drop across the sand sample or embankment [m]
L	length of seepage [m]
e	void ratio [-]
Q	flow rate [m^3/s]
Re	Reynolds number [-]
Re*	particle or grain Reynolds number [-]
u*	shear velocity [m/s]
Cu	uniformity coefficient (d_{60}/d_{10}) [-]
v	horizontal flow velocity [m/s]
x	horizontal direction
z	vertical direction
γ'_p	submerged unit weight of particles [N/m^3]
η	White's packing coefficient [-]
θ	bedding angle of sand [degrees]
μ	dynamic viscosity of the fluid [kg/m/s]
ρ_s	particle density [kg/m^3]
ρ_w	water density [kg/m^3]
τ	shear stress [kg/m^2]

φ hydraulic head in the pipe [m]

Ψ_c Shields parameter

subscripts

avg average

c critical

eq equivalent

max maximum

min minimum

w wall

1. Introduction

Internal erosion occurs when soil particles in an embankment dam or its foundations are carried downstream by seepage flow. There are four types of internal erosion: concentrated leak erosion, backward erosion, internal instability, and contact erosion (ICOLD, 2017). In granular soils with a cohesive and relatively impervious roof, backward erosion piping is the most likely failure mechanism to occur. These conditions often are found in river dikes, such as those on the main rivers in the Netherlands, the United States, Italy, and China. In these river systems, backward erosion is known to have led to sand boils and dike failures during floods.

Backward erosion occurs when seepage causes sand grains to be transported to the downstream side of the structure, leading to the development of shallow pipes that form in an upstream direction, while depositing eroded material on the downstream side of the structure. The pipes develop at the interface of the water transporting porous medium and an impermeable cohesive layer, since the latter forms the roof above the pipes and facilitates the large hydraulic gradients required for pipe initiation and progression. One pipe or a pattern of pipes will form in the upstream direction, and, when a pipe reaches the upstream side, the continuous flow may cause the pipe to widen and deepen to such an extent that the water-retaining structure becomes unstable.

Since the turn of the last century, the process of piping has been studied in the context of weir and dam design. Clibborn (1902) was the first to establish a linear relation between the length of seepage (L) and the critical head (H) across the structure (L = CH). Bligh (1910) embraced this idea and established coefficients of percolation (C) to predict safe values for hydraulic head on the basis of weirs in India. More recent approaches take other influential factors into account as well, such as the shape of the porous medium and sand characteristics. Using the results of laboratory investigations, Sellmeijer (1988) and Schmertmann (2000) each developed a quantitative theory for describing the process of piping, thereby including these influential factors. The theory of Sellmeijer (1988) is a physics-based solution that solves the coupled groundwater – erosion phenomenon for a specific levee (dike) configuration, taking account of the two dimensional flow towards the pipe, the viscous flow in the pipe, and the equilibrium of particles at the pipe's bottom. The theory developed by Schmertmann (2000) requires laboratory measurements of the critical gradients and relies on the user to interpret the site specific seepage regime for any field scenario.

Both Schmertmann's (2000) model and Sellmeijer's (1988) model rely on calibration with the critical heads observed in experiments. This is not an issue as long as the simulated conditions in practice are similar to those in the experiments by which the model was calibrated (e.g., homogeneous soil and similar exit conditions). However, when conditions in practice are different from those in the laboratory, the calibrated model no longer predicts the value correctly (for example, as illustrated by Van Beek et al. (2015) for three dimensional exits). Therefore, there is a need to describe the involved processes in closer resemblance to reality.

In Germany, Hanses (1985) studied the process of piping in detail and stated that the progression of a pipe depends on primary erosion (erosion at the pipe tip) and on secondary erosion (erosion at the pipe walls and bottom, which define the width and depth of the pipe). Van Beek et al. (2015) recently found evidence supporting this approach as well. To be able to predict pipe progression it is essential to understand the hydraulic conditions in the pipe as the pressure in the pipe determines the Darcyan flow towards the pipe from the foundation as well as the local hydraulic gradient upstream of the pipe causing pipe progression. The depth of the pipe is generally small (on the order of millimeters), since the flow through the pipe is provided by the flow through the porous medium, and the flow that can be conveyed through the pipe increases rapidly with increase in depth. The size of the pipe is controlled by the

erosion of its bed and walls due to flow through the pipe and towards the pipe. Given the small dimensions, the flow is generally assumed to be laminar.

In the current paper, whether literature data on incipient motion in laminar flow can be used to determine the pipe dimensions and corresponding hydraulic conditions in the erosion pipes is assessed. This is accomplished by considering existing approaches for determining critical shear stresses of sands in laminar flow in computations of equilibrium pipe dimensions and corresponding pipe hydraulics. The theoretical values are compared to measurements from backward erosion experiments (cylindrical tests) done at the U.S. Army Engineer Research and Development Center (ERDC) that allowed for the investigation of the hydraulic conditions in the erosion pipes. The obtained incipient motion data from the piping experiments were compared to data from the literature.

2. Existing approaches for incipient motion in laminar flow

Sellmeijer (1988) was the first to incorporate incipient motion concepts in a backward erosion piping model. He modeled the pipe flow, assuming it is 2D and laminar, and defined the particle equilibrium at the bottom of the erosion pipe using the approach by White (1940). Based on the equilibrium of forces, a formulation of the critical wall shear stress (τ_c) was defined as:

$$\tau_c = \eta \frac{\pi}{6} \gamma_p^{'} d \tan\theta \tag{1}$$

in which $\gamma_p^{'}$ is the unit weight of submerged particles, d is the representative grain size, θ is the 'bedding angle' indicating the angle of repose of a single grain resting on two other grains at the pipe's bottom, which was used as a calibration parameter in large-scale backward erosion piping experiments (Silvis, 1991) and set to a constant value of 37 ° in practice (Sellmeijer et al., 2011). The packing coefficient (η) was set to a conservative value of 0.25 based on the experiments done by White (1940), although 0.30 provides a closer match to the experimental values found by White (1940).

In hydraulic engineering, the critical Shields parameter (Shields, 1936), Ψ_c, is often used for assessment of incipient motion and is a function of the particle Reynolds number, Re^*:

$$\Psi_c = \frac{\tau_c}{\gamma_p' d} = f\left(\frac{\rho_w u^* d}{\mu}\right) \quad (2)$$

in which u^* is the shear velocity, ρ_w is the water density, and μ the dynamic viscosity of the fluid. Combining Eqs. 1 and 2 shows the relation between the Shields parameter and the bedding angle:

$$\Psi_c = \eta \frac{\pi}{6} \tan\theta \quad (3)$$

The Shields parameter has been determined for a large variety of soil bed conditions; although in most cases the flow in the flume was turbulent.

Generally, the Shields parameter is determined in a flume with dimensions that far exceed those of the erosion channels typical for backward erosion piping. Since the Reynolds number is linearly related to the water depth, the flow in the flume is normally turbulent for incipient grain motion. When the particles are relatively small by comparison with the thickness of the laminar sub-layer, the flow around the grain is laminar (when Re < 3.5 (Chien & Wan, 1999)). Yalin and Karahan (1979), who did experiments in fully laminar flows, state that the thickness of the laminar sub-layer does not affect incipient motion: the critical wall shear stress is the same in fully laminar flows and in turbulent flows with grains shielded by the laminar sub-layer. The results obtained in larger flumes, but with grains shielded in the laminar sub-layer, can, therefore, be used to predict the initiation of motion in fully laminar conditions, as is expected to be the case with piping channels. Other researchers used a small water depth or a viscous fluid to ensure laminar conditions in the flume.

Experiments on incipient motion in laminar flow (due to the presence of a laminar sub-layer, a small water depth, or the use of a viscous fluid) have been described in White (1940), Ward (1968), White (1970), Mantz (1977), Yalin and Karahan (1979), Govers (1987), Loiseleux et al. (2005), and Ouriemi et al. (2007). Table 1 lists an overview of these experiments.

Mantz (1977) presented a formulation for the critical Shields parameter derived for laminar flow around a grain (valid for particle Reynolds numbers (Re^*) of 0.03–1) on the basis of the experiments described by White (1970) and his own additional experiments:

$$\Psi_c = 0.1\mathrm{Re}^{*-0.3} \tag{4}$$

All of these measurements were made in situations that differ from the conditions observed in pipes formed by backward erosion. In particular, pipes formed by backward erosion are very shallow erosion channels which have a high relative roughness. Additionally, these pipes have moveable beds on three of the four channel walls. These differences make it questionable to directly apply the literature incipient motion data to backward erosion piping computations. In the following sections, the usefulness of traditional incipient motion data for backward erosion piping computations is assessed through comparison with measurements obtained from piping experiments.

3. Cylinder tests

The conventional test equipment to assess backward erosion piping is a rectangular box filled with sand with either a slope, ditch, hole or plane type exit and a transparent cover (among others De Wit, 1984; Hanses, 1985; Robbins et al., 2016; Silvis, 1991; Townsend et al., 1988; Van Beek et al., 2011; Vandenboer et al., 2014), in which the sand bed is subjected to a horizontal hydraulic gradient until piping occurs. Although this set-up has the advantage of allowing the pipe to migrate laterally to find the weakest path, the drawback is that hydraulic conditions cannot be assessed easily as it is unknown where, precisely, the pipe will develop.

To assess the hydraulics near and in the pipe a fundamentally different type of experiment was developed at the ERDC laboratory in which the hydraulic conditions required for particle movement were explicitly measured by the instrumentation. The new type of laboratory piping test apparatus was designed as shown in Fig. 1, consisting of a horizontal tube instrumented with ports for pore pressure readings along the top and bottom. The cylindrical design ensures that a pipe will form directly beneath the pore pressure transducers along the top of the tube. This will allow for the assessment of hydraulic conditions in a pipe at equilibrium conditions. Since the pipe is located underneath

the pressure transducers the head drop in the pipe can be measured. Combining the head drop in the pipe to the measured flow velocity, allows for determination of the critical shear stress. By running these experiments at different scales (tube diameters of 2.54 cm (tube A), 7.62 cm (tube B), and 15.24 cm (tube C)), the critical shear stress could be assessed at different flow rates in the pipe. Details with respect to the set-up, preparation method, observations during the experiments, and obtained critical gradients are published in Robbins et al. (2018).

The tests were done with 40/70 sand (sieved sand fraction between the No. 70 and No. 40 standard U.S. sieve sizes (0.212-0.425 mm)) and 20/40 sand (sieved sand fraction between the No. 40 and No. 20 standard U.S. sieve sizes (0.425-0.850 mm)), for which the characteristics are listed in Table 2. The water temperature was measured in the upstream water tank and was approximately 20 °C in each test.

The tests were done by gradually raising the gradient across the tube until pipe-formation took place. If the upstream head is maintained at a constant level after initial pipe formation, the pipe will continue to develop towards the upstream side, since the head drop required for initiating the pipe exceeds the head drop required to cause pipe progression (Robbins et al., 2018). However, when the pipe is continuously developing, there is no opportunity to measure the hydraulic conditions in the pipe, required for analysis of the particle equilibrium. Therefore, the pipe formation was stopped by lowering the head gradually as soon as the pipe reached halfway through the tube, to be able to search for particle equilibrium conditions. When the pipe formation had ceased, the head was gradually applied again, until limited particle movement at the bed was observed visually, indicating incipient motion conditions. At this point, at which the pipe was at or below the gradient required for pipe progression, the upstream head was maintained at a constant level, such that the (average) pipe gradient could be reliably measured using the pore pressure transducers. In addition, the maximum flow velocity in the pipe could be measured by injecting a limited amount of dye into the most upstream port in the pipe, which did not affect the stable conditions in the pipe. Subsequently, the head was gradually increased and the pipe was allowed to progress fully and erode until particle equilibrium conditions were obtained in the eroded pipe. At this stage, the average pipe gradient was measured manually by connecting the ports to riser tubes near the beginning and end of the tube, and dye was injected again for measuring the maximum flow velocity. After this measurement, the head was increased, and the procedure for measuring critical wall shear stress conditions was repeated in order to obtain more details on incipient erosion in slightly deeper pipes.

For every injection, it was found that the dye followed the streamlines precisely, indicating laminar flow in the pipe (Fig. 2). In one of the experiments, the depth of the pipe was measured along its length using a point laser. The depth was determined based upon polynomial fits of the series of point measurements along the top of the sample before and after full pipe development, in equilibrium with the applied head for a test done with 20/40 sand. The depth along the column was approximately 4-5 mm, with an average depth of 4.7 mm which is equal to approximately 8 times the mean grain diameter (more details on the point laser measurements are described in Robbins et al. (2018).

4. Incipient motion analysis for cylinder experiments

The critical wall shear stress can be determined by calculating the shear stress exerted by the flow on the particles through the pipe with the particles in limit-state conditions. The wall shear stress is a function of the velocity profile and is defined as:

$$\tau_w = \mu \left. \frac{\partial v}{\partial z} \right|_{wall} \tag{5}$$

where v is the horizontal local velocity in the pipe and z is the vertical direction from the bottom wall. Assuming laminar flow, the velocity profile can be determined using viscous flow equations. The Sellmeijer (1988) model assumes laminar flow in the pipe, and, since the model is 2D, an infinitely wide pipe, for which the wall shear stress is defined as:

$$\tau_w = h \frac{\rho_w g}{2} \frac{\partial \varphi}{\partial x} \tag{6}$$

in which h is the pipe depth, g the gravitational acceleration, φ the hydraulic head in the pipe, and x is the direction along the pipe. However, this equation is not appropriate for determining the wall shear stress in the cylinder experiments, since in the cylinders the pipe is not infinitely wide and the top of the pipe is curved. The most suitable shape for determining the flow is that of an ellipse, for which Lekner (2007) provides an equation. The horizontal flow velocity (v) in the ellipse, with the radius a in z-direction and b in y-direction (Fig. 3) is:

$$v = v_{\max}\left(1-\frac{y^2}{b^2}-\frac{z^2}{a^2}\right) \tag{7}$$

Lekner (2007) also provides equations relating the hydraulic gradient in the pipe ($\partial\varphi/\partial x$), flow ($Q$), and maximum velocity (v_{max}) in the pipe:

$$v_{\max} = \frac{2Q}{\pi ab} \tag{8}$$

and:

$$Q = \frac{\pi}{4\mu}\rho_w g\frac{\partial\varphi}{\partial x}\frac{(ab)^3}{\left(a^2+b^2\right)} \tag{9}$$

By differentiating Eq. 7 with respect to z, and substituting Eqs. 8 and 9, the wall shear stress can be determined for ellipse-shaped pipes, as a function of the hydraulic gradient in the pipe and pipe dimensions:

$$\tau_w = \mu\left.\frac{\partial v}{\partial z}\right|_{z=-a} = \frac{2}{a}\mu v_{\max} = \rho_w g\frac{\partial\varphi}{\partial x}\frac{b^2 a}{\left(a^2+b^2\right)} \tag{10}$$

It can easily be seen that for larger ratios of b to a the equation for the wall shear stress in an ellipse simplifies to the equation for parallel plates (Eq. 6). As will be confirmed later, this simplification is allowed for pipes formed by backward erosion, which have large width to depth ratios. The calculation of the wall shear stress normally requires the pipe depth, which is difficult to precisely determine since it is very small (on the order of a few to a few tens of grain diameters). An alternative way to calculate the wall shear stress is to make use of the maximum velocity instead of the pipe depth, this approach is used in the current paper. The maximum velocity, as a function of the hydraulic gradient in the pipe, material properties, and pipe dimensions, is obtained by combining Eqs. 8 and 9. After simplification for the large width-to-depth ratio, Eq. 11 is obtained:

$$v_{\max} = \frac{\rho_w g}{2\mu}\frac{\partial\varphi}{\partial x}\frac{(ab)^2}{\left(a^2+b^2\right)} \approx \frac{\rho_w g}{2\mu}\frac{\partial\varphi}{\partial x}a^2 \tag{11}$$

Substituting *a* in Eq. 10 using Eq. 11, an equation for wall shear stress based on the hydraulic gradient and maximum velocity is obtained, which is used to calculate the wall shear stress in the experiments under critical conditions:

$$\tau_w = \sqrt{\rho_w g \frac{\partial \varphi}{\partial x} v_{\max} 2\mu} \tag{12}$$

5. Results

Tables 3 and 4 list the measured hydraulic gradient in the pipe and maximum velocity, and the calculated particle Reynolds numbers, Reynolds numbers, pipe depths, critical shear stresses, critical Shields parameters, and bedding angles for all available incipient motion tests, for the pipes halfway through the tube and the fully developed pipes, respectively. No results from tube A are available, since this tube was found to be too small to successfully initiate backward erosion piping (Robbins et al., 2018). The pipe depth was calculated using Eq. 11. The particle Reynolds numbers (Re^*) and Reynolds numbers (Re) were calculated using Eqs. 13 and 14, in which d_{50} is the particle diameter for which 50% of the sample is finer, u^* is the shear velocity and v_{avg} is the average velocity. Equation 14 gives the Reynolds number for parallel plates, with a hydraulic diameter of $2h$. For an ellipse, the hydraulic diameter would be slightly smaller, approximately $1.5h$ for width to depth ratios of 10 (Fay, 1998), which means that the Reynolds number is slightly overestimated. The laminar flow in the pipe was confirmed by the calculated Reynolds numbers, which did not exceed the critical Reynolds number of 2800 for parallel plates (Fox et al., 2009).

$$\mathrm{Re}^* = \frac{\rho_w u^* d_{50}}{\mu} \text{ with } u^* = \sqrt{\frac{\tau_w}{\rho_w}} \tag{13}$$

$$\mathrm{Re} = \frac{2\rho_w v_{avg} h}{\mu} \text{ with } v_{avg} = \frac{v_{\max}}{2} \tag{14}$$

The Shields parameters were translated to bedding angles for comparison with the applied bedding angle in the Sellmeijer (1988) model, using a value of η of 0.3 and Eq. 3.

The critical wall shear stresses for 40/70 sand were obtained for samples with different void ratios. No correlation was observed between void ratio and critical wall shear stress (Fig. 4). It can be concluded that the influence of the void ratio on critical wall shear stress is minor compared to the scatter.

The obtained critical wall shear stresses were relatively low for some of the pipes halfway through the tube (Fig. 4) compared to most values found for fully-developed pipes. The fact that the partially developed pipe is not a pipe at natural equilibrium may explain these low critical wall shear stresses. Although the head was lowered gradually to cease the development of the pipe halfway through the tube, particles may have been deposited in the pipe, creating a slightly irregular surface. The consequent local onset of particle movement that was observed when the head was gradually raised may not be representative for the entire pipe. For the fully developed pipes, the critical wall shear stress was determined after natural equilibrium was established, resulting in higher values than for partially developed pipes.

The calculated depths listed in Tables 3 and 4 were used to confirm the large width to depth ratio as previously assumed. The average width (estimated from pictures)-to-depth ratio was found to be approximately 14, with a minimum of 9, indicating that the used approach is valid. For the only experiment in which the calculated depth could be compared to the measured depth (experiment 11B), since for this experiment the point laser was used to determine the average depth, a good agreement was found (the calculated depth was 4.3 mm and average depth determined with the laser was found to be 4.7 mm).

The pipes encountered in backward erosion are relatively small (depth on the order of millimeters), so that it is usually assumed that the flow is laminar in the pipe. The cylindrical experiments confirm that the flow is laminar for the used sand types and configuration sizes.

6. Discussion

The experimentally obtained critical shear wall stresses in the pipes are plotted in the Shields diagram (Shields parameter as a function of the particle Reynolds number) for comparison with data from the literature (Fig. 5). The experiments on plastics described in Ward (1968) have been removed from the selection since the particle density was only slightly higher than the water density and are not considered representative for transport of sand grains.

White's theoretical formulation (1940), as applied with a constant bedding angle (θ = 37°) and the conservative coefficient η = 0.25 commonly used in the Sellmeijer model (Sellmeijer et al., 2011), also is shown in the graph. The formulation by Mantz (1977) and a full Shields curve as proposed by Cao et al. (2006) are added to the graph as well. In most test series, the critical Shields parameter decreases with increasing values of the particle Reynolds number, except in the case of Ouriemi et al. (2007), who concluded that the critical Shields parameter is constant in the laminar regime ($\Psi_c = 0.12 \pm 0.03$).

The Shields parameters obtained in the cylindrical tests are in the same range as the values obtained from the literature. The scatter in Shields parameters of the 40/70 sand is quite significant compared to the literature data. This is partly related to the lower values observed for the partially developed pipes.

By rewriting the particle Reynolds number in terms of particle diameter and using a constant value for viscosity, the effect of viscosity is taken into account, resulting in an 'equivalent diameter in regular viscosity conditions (T = 20 °C)':

$$d_{50,eq} = \frac{\mu \mathrm{Re}^*}{\rho_w u^*} \tag{15}$$

The Shields parameter can be expressed as proportional to the bedding angle using Eq. 3. The effect of particle diameter on critical wall shear stress and bedding angle is shown in Fig. 6. Clearly the bedding angle is not a constant as was applied in the Sellmeijer (1988) model, but depends on the Reynolds number, or for constant viscosity on particle diameter. For fine sands with diameters of approximately 0.2 mm, the value of 37°, as commonly applied for the Sellmeijer (1988) model, is close to the incipient motion data from the literature. The negative trend of bedding angle and particle size shown in Fig. 6 was also observed by Simons and Sentürk (1992), who related the angle of repose (determined by introducing particles of sediment into water with near zero velocity and measure the toe angle of the submerged cone of deposited sediment) to the incipience of motion in a similar way that White (1940) related the bedding angle to the incipience of motion and who observed a minimum angle of repose for a representative particle diameter of 1-2 mm. When the bedding angles from Fig. 6 and the angles of repose by Simons and Sentürk (1992) are compared, the angles of repose were found to be much larger (approximately by a factor of 3) in the graph of Simons and Sentürk (1992) than in Fig. 6, although the number of data points in Simons and Sentürk (1992) is limited (curve derived from a few data points of coarse sands with d > 6

mm and data points from other materials, i.e. lignite, Bakelite, and pumice). Altogether the incipient motion data in laminar flow are limited in the range of interest for application to backward erosion piping (0.1-1 mm).

The comparison of literature data to the current experiments illustrates that the particle equilibrium in pipes formed by backward erosion can be predicted using existing incipient motion criteria. In the current experiments, the flow in the pipe was laminar. However, it can be questioned whether the assumption of laminar flow still holds for larger particles, for which more research is required. Nevertheless, the findings illustrate that the incipient motion data can be used to predict the particle equilibrium, and, thereby, also the pipe depth and head loss in the pipe. This is an essential part of backward erosion modeling, since the head loss in the pipe directly influences the local hydraulic gradient at the pipe tip, which controls the progression of the pipe.

7. Conclusions

In this paper horizontal cylinder experiments are presented to validate the use of incipient motion data from the literature for modeling of backward erosion piping. The collected data, consisting of the heads in the erosion channel as well as the flow velocity, could be used to study incipient motion of particles in a pipe formed naturally by backward erosion. Calculated Reynolds numbers for flow through the pipes and visualized streamlines by dye injection showed that the flow was laminar in all investigated pipes. The obtained critical wall shear stresses, critical Shields parameters, and bedding angles, denoting the equilibrium of particles in the pipe, concur with the experimental values found in the literature for laminar flow. This indicates that the approach of determining the critical pipe gradient based on incipient motion data in laminar flow is valid and the bedding angle is not a constant, as was previously assumed in the calibration of the Sellmeijer model (Sellmeijer et al., 2011). Limited data on incipient motion are available in the literature for sands with $d_{50} > 0.5$ mm. It is recommended to determine the critical wall shear stress for coarser sands and check the assumption of laminar flow again. The findings can be used for further improvement of backward erosion piping models. The local hydraulic gradient near the pipe tip controls the progression of the pipe and is directly affected by the head loss in the pipe, which can now be determined using incipient motion data from the literature. Coupling of a criterion for the local hydraulic gradient at the tip and pipe hydraulics based on the particle equilibrium in the pipe is expected to lead to a more accurate description of the piping process compared to existing models.

Acknowledgements

This paper was produced as part of an international cooperation between the U.S. Army Corps of Engineers and Rijkswaterstaat, part of the Dutch Ministry of Infrastructure and the Environment. The authors express sincere gratitude to the U.S. Army Corps of Engineers and Rijkswaterstaat for this opportunity. The research presented is funded by the Dutch Government and the U.S. Army Corps of Engineers. Results are intended to be used in instruments for assessment and design of flood defenses. Permission to publish was granted by Director, Geotechnical and Structures Laboratory (U.S. Army Corps of Engineers).

References

Bligh,W.G. (1910). Dams barrages and weirs on porous foundations. *Engineering News*, 64(26), 708-710.

Cao, Z., Pender G., & Meng, J. (2006). Explicit formulation of the Shields diagram for incipient motion of sediment. *Journal of Hydraulic Engineering*, *132*(10), 1097-1099.

Chien, N., & Wan, Z. (1999). *Mechanics of sediment transport*. Reston, VA, U.S.: ASCE Press.

Clibborn, J. (1902). Experiments on the passage of water through sand. *Technical Paper No. 97*, Government of India. Roorkee, India.

De Wit, J.M. (1984). *Onderzoek zandmeevoerende wellen*. Rapportage Modelproeven. Grondmechanica Delft Report CO-220887/10. (*In Dutch*)

Fay, J.A. (1998). *Introduction to fluid mechanics*. MA, U.S.: MIT Press, Cambridge, Massachusetts.

Fox, R.W., Pritchard, P.J., & McDonald, A.T. (2009). *Introduction to fluid mechanics*. New York: John Wiley & Sons.

Govers, G. (1987). Initiation of motion in overland flow. *Sedimentology, 34*, 1157-1164.

Hanses, U. (1985). *Zur Mechanik der Entwicklung von Erosionskanälen in geschichtetem Untergrund unter Stauanlagen*. (*Ph.D. dissertation)*, Grundbauinstitut der Technischen Universität Berlin, Germany. (*In German*)

International Commission on Large Dams (ICOLD). (2017). *Internal erosion of existing dams, levees and dikes, and their foundations – Volume 1: Internal erosion processes and engineering assessment*. Bulletin 164. ICOLD. Paris, France.

Lekner, J. (2007). Viscous flow through pipes of various cross-sections. *European Journal of Physics, 28*, 521–527.

Loiseleux, T., Gondret, P., Rabaud, M., & Doppler, D. (2005). Onset of erosion and avalanche for an inclined granular bed sheared by a continuous laminar flow. *Physics of Fluids, 17*(103304), 1-9.

Mantz, P.A. (1977). Incipient transport of fine grains and flakes by fluids – Extended Shields diagram. *Journal of the Hydraulics Division, ASCE, 103*(HY6), 601-615.

Ouriemi, M., Aussillous, P., Medale, M., Peysson, Y., & Guazzelli, E. (2007). Determination of the critical Shields number for particle erosion in laminar flow. *Physics of Fluids, 19*(061706), 1-4.

Robbins, B.A., Montalvo-Bartolomei, A., López-Soto, J., & Stephens, I.J. (2016). Laboratory measurements of critical gradients of cohesionless soils. *Proceedings, 36th Annual U.S. Society on Dams Conference*, Denver, CO.

Robbins, B.A., van Beek, V.M., Lopez-Soto, J.F., Montalvo-Bartolomei, A.M., & Murphy, J. (2018). A novel laboratory test for backward erosion piping. *International Journal of Physical Modelling in Geotechnics, 18*(5), 266-279.

Schmertmann, J.H. (2000). The no-filter factor of safety against piping through sands. In: F. Silva & E. Kavazanjian, Jr., (Eds). *Judgment and innovation: ASCE Geotechnical Special Publication, 111*, 65–132. Reston, USA.

Simons, D.B., & Sentürk, F. (1992). *Sediment transport technology – water and sediment dynamics*. Highlands Ranch, CO, U.S.: Water Resources Publications.

Sellmeijer, J.B. (1988). *On the mechanism of piping under impervious structures*. (*Ph.D. dissertation)*, TU Delft, The Netherlands.

Sellmeijer, J.B., Lopéz de la Cruz, J., Van Beek, V.M., & Knoeff, J.G. (2011). Fine-tuning of the piping model through small-scale, medium-scale and IJkdijk experiments. *European Journal of Environmental and Civil Engineering, 15*(8), 1139-1154.

Shields, A. (1936). *Anwendung der Ahnlichkeitsmechanik und Turbulenzforschung auf die Geschiebebewegung. Mitteilungen der Preußischen Versuchsanstalt für Wasserbau und Schiffbau*, heft 26, Berlin. (*In German*)

Silvis, F. (1991). *Verificatie piping model: Proeven in de Deltagoot*. Grondmechanica Delft, Delft, The Netherlands. (*In Dutch*)

Townsend, F.C.D., Bloomquist, D., Shiau, J.M., Martinez, R., & Rubin H. (1988). *Evaluation of filter criteria and thickness for mitigating piping in sand*. University of Florida, Department of Civil Engineering, USA, report U.F. #4910450421512.

Van Beek, V.M., Knoeff, J.G., & Sellmeijer, J.B. (2011). Observations on the process of backward piping by underseepage in cohesionless soils in small-, medium- and full-scale experiments. *European Journal of Environmental and Civil Engineering*, *15*(8), 1115-1137.

Van Beek, V.M., Van Essen, H.M., Vandenboer, K., & Bezuijen, A. (2015). Developments in modelling of backward erosion piping. *Géotechnique*, *65* (9), 740-754.

Vandenboer, K., Bezuijen, A., & Van Beek, V.M. (2014). 3D character of backward erosion piping: Small-scale experiments. In L. Cheng, S. Draper, & H. An (Eds.), *Proceedings 7th International Conference on Scour and Erosion*, (pp. 81-86), London: Taylor & Francis Group.

Ward, B.D. (1968). *Surface shear at incipient motion of uniform sands*. (Ph.D. dissertation), University of Arizona, department of hydraulic engineering, Tucson, AZ.

White, C.M. (1940). The equilibrium of grains on the bed of a stream. *Proceedings of the Royal Society*, series A, *174*, 322-338.

White, S.J. (1970). Plane bed thresholds of fine grained sediments. *Nature, 228*(10), 152-153.

Yalin, M.S., & Karahan, E. (1979). Inception of sediment transport. *Journal of the Hydraulics Division, ASCE, 105*(HY11), 1433-1443.

Fig. 1 Set up showing the three tubes prior to sample preparation.

Fig. 2 Injected dye follows streamlines, confirming laminar flow conditions.

Fig. 3 Ellipse with contours at 0% (outer contour) to 90% (inner contour) of the maximum velocity.

Fig. 4 Effect of void ratio on critical shear stress in 40/70 sand.

Fig. 5 Shields parameter as a function of the particle Reynolds number showing experimental results for laminar flow (including the cylindrical tests), various fits, and theoretical relations.

Fig. 6 Critical shear stress and bedding angle as function of particle diameter.

Table 1 Overview of incipient motion for particles in laminar flow.

Source	Material	Mean grain size [mm]	Fluid
White (1940)	Sand	0.21 / 0.90	Oil
Ward (1968)	Sands / glass beads / taconite / plastics	0.240–2.29	Oil
White (1970)	Natural sands and silts / plastics / lead glass / crushed silica	0.016–2.2	Water / Oil
Mantz (1977)	Natural grains / crushed silica	0.015–0.066	Water
Yalin and Karahan (1979)	Sieved river sands	0.56–2.85	Glycerine / water mixture
Govers (1987)	Silt and quartz sands	0.045–1.098	Water
Loiseleux et al. (2005)	Glass beads	0.110–0.220	Water
Ouriemi et al. (2007)	Polystyrene / PMMA / glass spheres	0.132–0.538	Oil / water mixture

Table 2 Sand characteristics. (see List of Symbols for definition of terms)

Sand type	d_{50}	d_{60}	Cu	ρ_s	e_{min}	e_{max}
	[m]	[m]	[-]	[kg/m3]	[-]	[-]
40/70	3.00E-04	3.22E-4	1.42	2650	0.56	0.80
20/40	6.00E-04	6.45E-4	1.38	2650	0.52	0.75

Table 3 Incipient motion parameters for partial developed pipes up to half of the seepage length. (see List of Symbols for definition of terms)

Test number	d_{50}	Measured values			Calculated values					
		e	$d\varphi/dx$	v_{max}	Re*	Re	h	τ_c	Ψ_c	θ
	[m]	[-]	[-]	[m/s]	[-]	[-]	[m]	[Pa]	[-]	[degrees]
Test 3B	3.00E-04	0.68	0.093	0.057	5.4	40	7.1E-04	0.322	0.066	22.9
Test 3C	3.00E-04	0.61	0.062	0.083	5.3	87	1.0E-03	0.318	0.065	22.6
Test 4B	3.00E-04	0.63	0.098	0.098	6.3	88	9.0E-04	0.434	0.089	29.6
Test 4C	3.00E-04	0.64	0.080	0.114	6.2	123	1.1E-03	0.423	0.087	29.0
Test 8B	6.00E-04	0.51	0.027	0.147	10.0	310	2.1E-03	0.279	0.029	10.4

Table 4 Incipient motion parameters for fully developed pipes. (see List of Symbols for definition of terms)

Test number	d_{50}	Measured values			Calculated values					
		e	$d\varphi/dx$	v_{max}	Re*	Re	h	τ_c	Ψ_c	θ
	[m]	[-]	[-]	[m/s]	[-]	[-]	[m]	[Pa]	[-]	[degrees]
Test 2B-1	3.00E-04	0.64	0.035	0.315	6.5	853	2.7E-03	0.465	9.58E-02	31.4
Test 2B-2	3.00E-04	0.64	0.026	0.400	6.4	1417	3.5E-03	0.452	9.30E-02	30.6
Test 2B-3	3.00E-04	0.64	0.023	0.461	6.4	1864	4.0E-03	0.456	9.39E-02	30.9
Test 2C-1	3.00E-04	0.66	0.030	0.333	6.3	1002	3.0E-03	0.443	9.12E-02	30.1
Test 2C-2	3.00E-04	0.66	0.016	0.353	5.4	1515	4.3E-03	0.329	6.77E-02	23.3
Test 2C-3	3.00E-04	0.66	0.013	0.375	5.2	1855	4.9E-03	0.303	6.25E-02	21.7
Test 3B-1	3.00E-04	0.68	0.056	0.204	6.5	351	1.7E-03	0.474	9.77E-02	31.9
Test 3B-2	3.00E-04	0.68	0.045	0.248	6.5	526	2.1E-03	0.468	9.64E-02	31.5
Test 3B-3	3.00E-04	0.68	0.038	0.25	6.2	578	2.3E-03	0.432	8.91E-02	29.6
Test 3C-1	3.00E-04	0.61	0.053	0.187	6.3	317	1.7E-03	0.441	9.08E-02	30.0
Test 3C-2	3.00E-04	0.61	0.050	0.169	6.1	281	1.7E-03	0.407	8.39E-02	28.1
Test 3C-3	3.00E-04	0.61	0.039	0.271	6.4	645	2.4E-03	0.455	9.38E-02	30.8
Test 4B-1	3.00E-04	0.63	0.040	0.211	6.1	438	2.1E-03	0.407	8.38E-02	28.1
Test 4B-2	3.00E-04	0.63	0.037	0.242	6.1	561	2.3E-03	0.417	8.59E-02	28.7
Test 4B-3	3.00E-04	0.63	0.033	0.306	6.3	837	2.7E-03	0.447	9.21E-02	30.4
Test 4C-1	3.00E-04	0.64	0.053	0.117	5.6	156	1.3E-03	0.350	7.21E-02	24.6
Test 4C-2	3.00E-04	0.64	0.047	0.155	5.8	255	1.6E-03	0.377	7.76E-02	26.3
Test 4C-3	3.00E-04	0.64	0.051	0.153	5.9	239	1.6E-03	0.392	8.07E-02	27.2
Test 7B-1	3.00E-04	0.60	0.037	0.269	6.3	658	2.4E-03	0.440	9.06E-02	30.0
Test 8B-1	6.00E-04	0.51	0.020	0.197	10.0	558	2.8E-03	0.278	2.86E-02	10.3
Test 8B-2	6.00E-04	0.51	0.020	0.305	11.2	1076	3.5E-03	0.346	3.56E-02	12.8
Test 11B	6.00E-04	0.62	0.016	0.349	10.9	1483	4.3E-03	0.328	3.38E-02	12.1

Fig. 1.

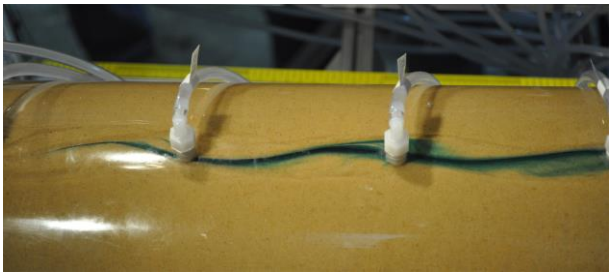

Fig. 2.

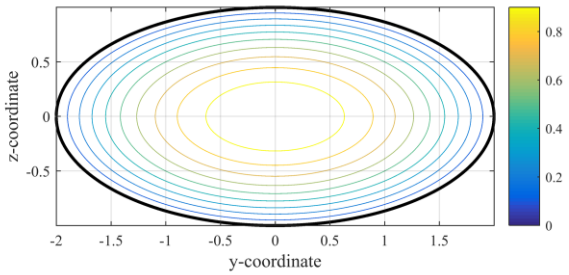

Fig. 4.

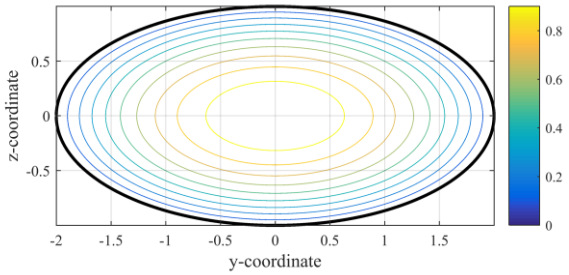

Fig. 4.

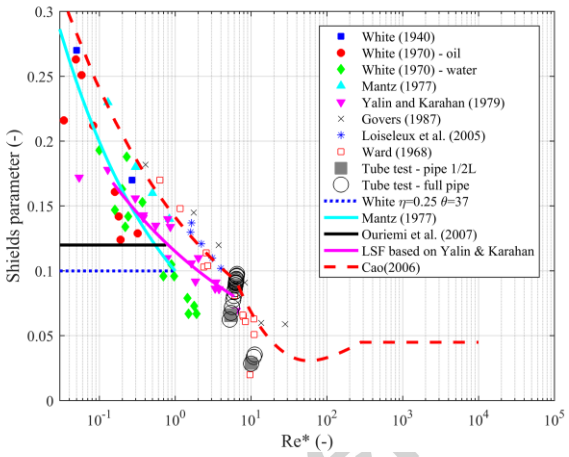

Fig. 5.

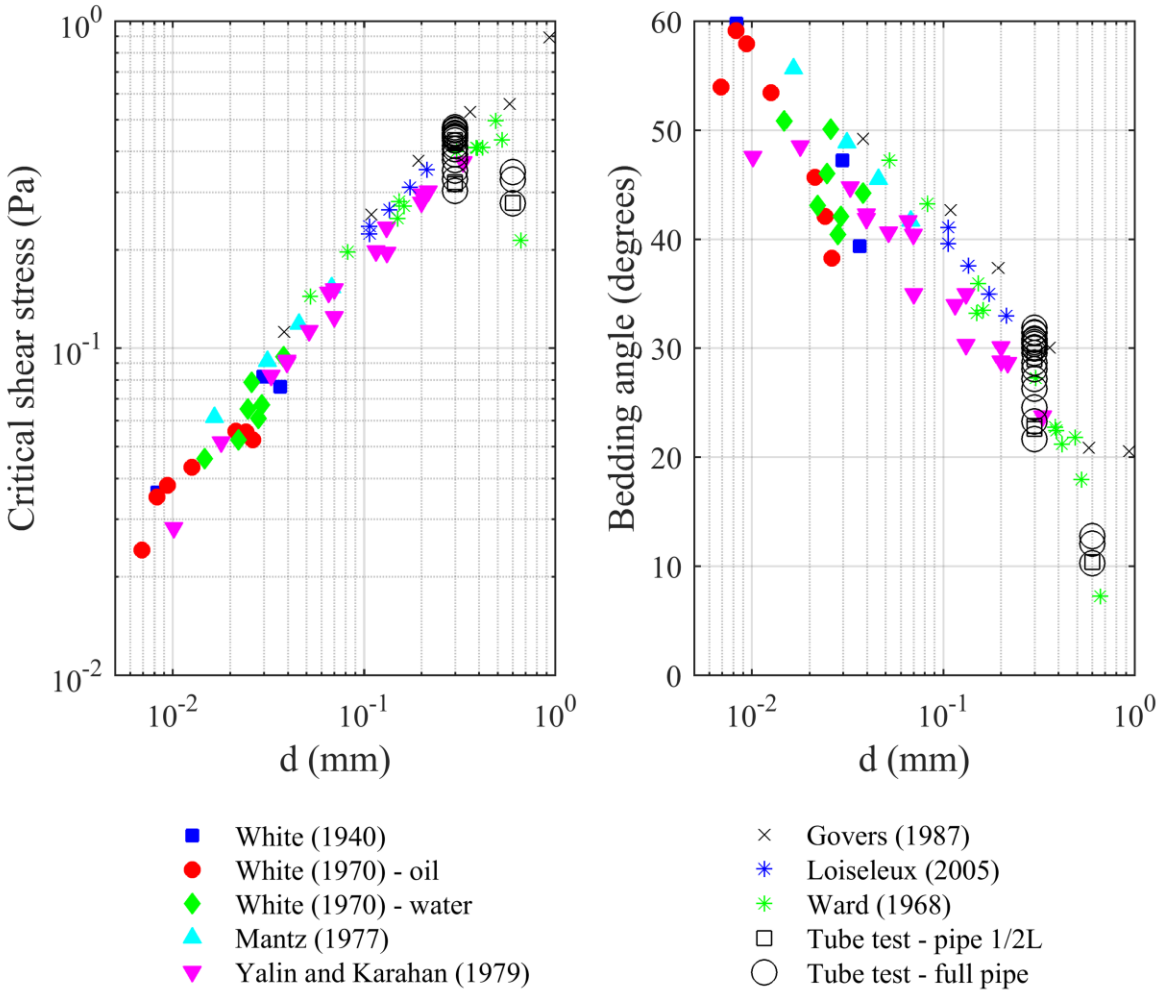
Critical shear stress (Pa)
d (mm)
Bedding angle (degrees)
d (mm)
White (1940)
White (1970) - oil
White (1970) - water
Mantz (1977)
Yalin and Karahan (1979)
Govers (1987)
Loiseleux (2005)
Ward (1968)
Tube test - pipe 1/2L
Tube test - full pipe

Fig. 6.